COMMUNICATION

# Phenylphosphonic acid as a grain-refinement additive for stable lithium metal anode

Received 00th January 20xx,
Accepted 00th January 20xx

DOI: 10.1039/x0xx00000x

Pinjuan Zou [a], Jun Liu [a], Zhenguo Huang*[b], Renzong Hu [a] and Liuzhang Ouyang*[ac]

**Phenylphosphonic acid (PPOA) has been proposed as a new additive for carbonate electrolyte, in which the complexation reaction between PPOA and $Li^+$ reduces the nucleus size and boosts nucleation quantity during the plating process. Thus, enhanced cycling stability is obtained in both symmetric cells and full cells.**

With an ultrahigh theoretical capacity (3860 mAh $g^{-1}$) and the lowest redox potential (-3.04 V versus standard hydrogen electrode), lithium (Li) metal has been regarded as the ideal anode for rechargeable lithium metal batteries (LMBs)[1-4]. The successful use of Li metal anode can not only significantly increase the energy density of the existing lithium-ion batteries (LIBs), but also help to advance Li-S and Li-air battery technologies[5-7]. However, the application of Li metal anodes in LMBs has been impeded by the following hurdles. First, Li metal can continuously react with the electrolyte, which leads to the formation of ultra-thick solid electrolyte interphase (SEI) layer, therefore increasing the internal resistance and gradually decreasing the coulombic efficiency[8-10]. Second, the continuous volume change of Li metal during the stripping/plating processes brings in poor interfacial stability of the Li metal/electrolyte, which deteriorates the cycling performance[11, 12]. Third, the inhomogeneous deposition and the dendrite formation can puncture the separator, resulting in internal short circuit, overheating or even fires[13].

To conquer these problems, extensive efforts have been devoted to stabilizing the Li metal anodes, including adjusting electrolyte compositions[14, 15], building artificial protection layers on Li metal anode[16-20], designing three-dimensional current collectors[21], using solid-state electrolytes[22, 23] and so on. Among all the proposed approaches, tuning electrolyte component is the simplest strategy owing to its cost effectiveness and high compatibility with the existing battery industry[24]. Especially, electrolyte additives are deemed to be "vitamin" in the LIBs and play a particular role in improving electrochemical performances with less than 5% by volume or weight. In the stripping/plating processes, electrolyte additives can regulate the deposition behavior of Li metal and restrain dendritic Li formation. Some additives, such as vinylene carbonate[25] and fluoroethylene carbonate[26], can react with Li metal to generate a stable artificial solid-electrolyte interface (SEI) layer, suppressing the continuous side reactions between Li metal and the electrolyte. Some other additives, such as cesium ions[27] and hexadecyl trimethylammonium chloride[28], can aggregate around protuberances *via* electrostatic attraction and homogenize the deposition. Despite these encouraging achievements, it is still highly challenging to completely suppress Li dendrite formation, and the exploration of new electrolyte additive for this purpose is highly desirable.

Grain refinement has long been regarded as the most effective and the simplest approach to regulate the metal deposition behavior in the fields of copper electro-refining and electro-deposition, in which an increasing number of nuclei with uniform distribution can facilitate a homogeneous deposition. According to the equation of critical nucleus radius (equation 1), a high over-potential of electrochemical reaction can reduce the radius of metal nuclei and boost the number of nucleation sites.

$$\boldsymbol{r_k} = \frac{\sigma}{\rho F M^{-1} \Delta \varphi_K} \quad (1)$$

where $r_k$, $\Delta\varphi_K$, $\sigma$, $\rho$, F, $M$ are critical nucleus radius, over-potential, interfacial tension between anode and electrolyte, the density of nucleus, Faraday constant, molar mass, respectively. Therefore, the Li dendrite can also be suppressed through boosting the number of nucleation sites and reducing the Li nucleus size. For example, succinic anhydride and octaphenyl polyoxyethylene have been proposed as electrolyte additives to control the Li nucleus size and increase the number

[a] *School of Materials Science and Engineering and Key Laboratory of Advanced Energy Storage Materials of Guangdong Province, South China University of Technology, Guangzhou, 510641, People's Republic of China.*
Email: msouyang@scut.edu.cn
[b] *School of Civil and Environmental Engineering, University of Technology Sydney, Sydney, NSW, 2007 (Australia).*
Email: zhenguo.huang@uts.edu.au
[c] *China-Australia Joint Laboratory for Energy & Environmental Materials and Key Laboratory of Fuel Cell Technology of Guangdong Province, Guangzhou 510641, People's Republic of China.*
Electronic Supplementary Information (ESI) available: [details of any supplementary information available should be included here]. See DOI: 10.1039/x0xx00000x

of nucleation sites.[13, 29, 30] Relatively speaking, there are still very few electrolyte additives that can effectively regulate the nucleation quantity and the nucleus size for LMBs.

PPOA has been widely used to selectively extract $Li^+$ from aqueous solutions containing $Li^+$, $Na^+$ and $K^+$. The coordination reaction between $Li^+$ and PPOA inspires us to introduce PPOA as an additive in ester electrolyte to suppress the formation of Li dendrite. Owing to the coordination reaction between PPOA with $Li^+$ from $LiPF_6$, which was demonstrated by the nuclear magnetic resonance (NMR) and Fourier transform infrared spectroscopy (FTIR) analysis, PPOA can be dissolved in the $LiPF_6$-EC: DMC: EMC electrolyte (denote as BE). The introduction of PPOA can increase the over-potential of Li stripping/plating, reduce the nucleus size and boost the number of nucleation sites. As a result, carbonate electrolyte containing 0.5 wt% PPOA additive (marked as BE-PPOA) renders 400 h cycling at a current density of 0.5 mA $cm^{-2}$ with a Li utilization of 5 % in the Li||Li symmetric cells. Besides, the $Li_4Ti_5O_{12}$||Li full cells delivered greatly enhanced cycle stability at a high current density of 5 C.

As a common coordination agent used for extracting $Li^+$ from aqueous solutions, PPOA is easily dissolved in water but insoluble in the mixed solvents of EC, DMC and EMC (1:1:1 by volume), which is demonstrated by the white PPOA particles appearing at the bottom (Figure 1a). As shown in Figure 1b, PPOA was rapidly dissolved after adding $LiPF_6$ salt into the above solvent mixture likely because of the coordination reaction between PPOA and $Li^+$. The solubility of PPOA in the $LiPF_6$-EC: DMC: EMC can be as high as 4.0 wt%. The coordination reaction between PPOA and $Li^+$ will produce $H^+$, which leads to the formation of gray surface on Li foil after being immersed in the PPOA-containing electrolyte (Figure S1a and S1c). Decomposition products of electrolyte are observed by energy dispersive spectrometry (EDS) analysis of Li metal surface after immersing in BE-PPOA (Figure S1e-i). $^{19}F$ nuclear magnetic resonance (NMR) spectroscopy measurement confirms that the introduction of PPOA can increase the amount of HF and $PO_2F_2^-$ in BE-PPOA (Figure S2). In contrast, the Li foil maintains its metal luster after being immersed in the BE (Figure S1b and S1d). NMR analysis was carried out to explore the chemical environment of solvents and $Li^+$. Using $^{13}CDCl_3$ as the reference (Figure S3), the $^{13}C$ NMR spectra indicate that the introduction of PPOA has no profound effect on the chemical environment of the functional groups in the electrolyte (Figure S4 and S5). Compared with BE, the chemical shift of $^7Li$ in BE-PPOA experiences a downfield shift (Figure 1c), suggesting the strong complexation between PPOA additive and $Li^+$ [31]. FTIR and Raman spectra were also used to analyze the electrolytes. The nearly identical FTIR and Raman spectra of BE and PPOA-BE (Figure S6) indicate that the introduction of PPOA does not greatly change the molecular structure. Meanwhile, the peaks at 715.7 and 740.2 $cm^{-1}$ can be attributed to free EC solvent and the P-F symmetric stretching vibration of $PF_6^-$ (Figure 1d), which can be supported by the Raman spectra of BE and the mixed solvents of EC, DMC and EMC (1:1:1 by volume, Figure S7). Notably, the Raman peak of P-F symmetric stretching vibration experiences a blue shift, indicating the formation of more complexes between Li ions and $PF_6^-$ anions or more contact ion pairs (CIP)[32, 33], which is caused by the coordination between PPOA with $Li^+$ ions.

*In-situ* optical microscopy was first used to investigate the effect of PPOA additive on the behavior of $Li^+$ plating in the Li||Li symmetric cells at a current density of 1 mA $cm^{-2}$ and capacity of 1 mAh $cm^{-2}$. As displayed in Figure 1e, $Li^+$ deposition in BE is inhomogeneous and Li dendrites are visible on the Li foil after 6 minutes. The uncontrollable growth of Li dendrites becomes more pronounced after 12 minutes. In sharp contrast, the introduction of PPOA effectively suppressed the formation of Li dendrites in the whole plating process (Figure 1f). Even after deposition for 12 minutes, Li dendrites are invisible on the Li foil, illustrating the PPOA can refine the grains and regulate

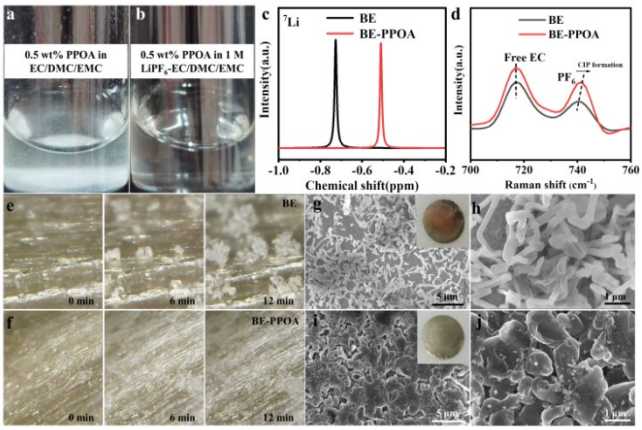


**Figure 1.** The digital photos of PPOA in (a) EC:DMC:EMC and (b) $LiPF_6$-EC:DMC:EMC. (c) $^7Li$ NMR spectra in BE and BE-PPOA. (d) Raman spectra of BE and BE-PPOA. *In-situ* optical microscopy photos of Li deposition process in (e) BE and (f) BE-PPOA at a current density of 1 mA $cm^{-2}$ and capacity of 1 mAh $cm^{-2}$. SEM images of the copper foil after Li deposition for 1 mAh $cm^{-2}$ in (g, h) BE and (i, j) BE-PPOA.

the Li deposition. Scanning electron microscopy (SEM) was also applied to investigate the detailed morphology of plated Li on Cu foil. After plating for 1 h at a current density of 1 mA $cm^{-2}$ in the Li||Cu cell in BE electrolyte, plated Li crystals are randomly distributed on the Cu surface (Figure 1g). Besides, the deposited Li presents fiber-like morphology (Figure 1h), which has large surface areas and therefore accelerate reactions between Li metal and the electrolyte. In contrast, the plated Li metal in PPOA-BE is dense and uniformly distributed on the Cu foil (Figure 1i, j). These large Li particles have much smaller surface areas and thus reduced reaction between Li metal and the electrolyte. Such difference indicates that PPOA additive can effectively regulate the uniformity and the morphology of Li nucleation, leading to dendrite-free growth of the Li deposition.

The effects of the PPOA loading amount on the electrochemical performances were evaluated in Li||Li symmetric cells (Figure S8). For the 0.5% loading, Li metal anode demonstrates the best cycling performance (Figure S8b). With a lower (0.25 wt%) or higher (1 wt%) loading, the output voltage is not steady. For the lower loading, there are not enough complexation reactions between PPOA and $Li^+$, so the Li plating cannot be effectively regulated (Figure S8a). With 1 wt% PPOA addition, the overpotential is much larger due to extensive complexation (Figure S8c). The viscosity of the electrolyte also increases with the increase of PPOA loading, as demonstrated

by the larger contact angle after adding 1 wt% PPOA in BE (Figure S9a, S9b) [30]. With a 0.5 wt% PPOA loading, the Li||Li symmetric cells can undergo stable stripping/plating for more than 400 h at a current density of 0.5 mA $cm^{-2}$ and a capacity of 0.5 mAh $cm^{-2}$ (corresponding to a Li utilization of 5%, Figure 2a). In contrast, the voltage polarization of the Li||Li symmetric cell in BE shows a gradual increase from 170 hours due to the continuous side reaction between Li dendrites and electrolyte.

The over-potential in BE-PPOA is higher than that in BE for the initial cycles (Figure 2c), which can be ascribed to the complexation between $Li^+$ and PPOA. This means that the reduction of coordinated $Li^+$ requires a more negative potential in BE-PPOA. The elevated electro-deposition over-potential can boost the number of nucleation sites and promote the formation of small crystals, thus inducing a uniform and dense Li deposition layer. After several cycles, the over-potential of the cell with BE-PPOA is stabilized at 40 mV (Figure 2d), which is likely due to the formation of a stable SEI film. However, the cell in BE shows a higher over-potential in the following striping/plating processes, which can be attributed to the gradually increasing thickness of the SEI film. When the capacity was increased to 1 mAh $cm^{-2}$, the cells with PPOA-BE can maintain a stable cycling for 320 h, while the cell in BE is cycled for only 105 h before short circuit occurred (Figure 2b). The PPOA additive shows a strong stabilization capability for Li metal anodes even at a higher current density and deposition amount. When both the current density and deposition amount are increased to 1 mA $cm^{-2}$ and 1 mAh $cm^{-2}$, respectively, the polarization voltage in BE shows a significant increase after 35 h, while the symmetric cells with PPOA-BE delivers a stable cycle performance more than 150 h (Figure S8b).

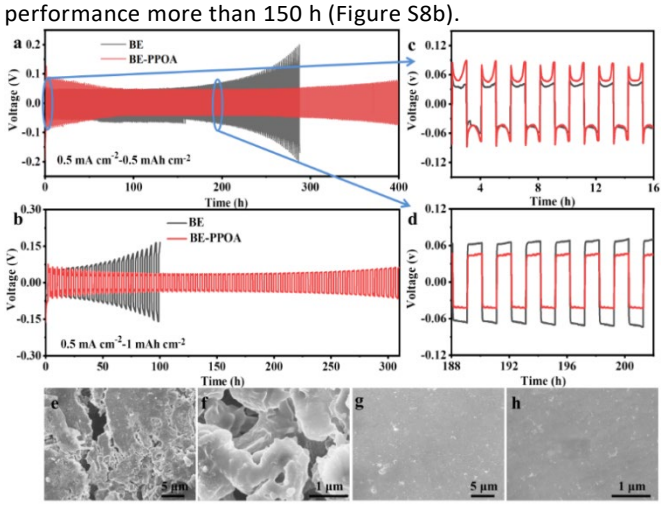


**Figure 2**. Cycle stability the Li||Li symmetric cells at a current density of 0.5 mA $cm^{-2}$ with a capacity of (a) 0.5 mAh $cm^{-2}$ and (b) 1 mAh $cm^{-2}$ in BE and PPOA-BE. (c) the initial 8 cycles and (d) 94-101 cycles. SEM images of Li foils after 50 cycles in (e, f) BE and (g, h) BE-PPOA at a current density of 1 mA $cm^{-2}$ and a capacity of 1 mAh $cm^{-2}$.

SEM was used to observe the Li metal anode surface after 50 cycles in BE and BE-PPOA in Li||Li symmetric cells. The Li metal anode cycled in BE exhibits a loosely packed and porous structure (Figure 2e, f). In sharp contrast, the Li metal anode cycled in BE-PPOA displays a smooth surface (Figure 2g, h), suggesting a remarkably improved uniformity of Li deposition. The electrochemical impedance spectroscopy (EIS) measurement of the Li||Li cells in BE-PPOA also shows improved interfacial stability. The cell after 2 cycles in BE-PPOA shows a higher charge transfer resistance ($R_{ct}$) owing to the complexation reaction between $Li^+$ and PPOA (Figure S10). After 10 cycles, $R_{ct}$ is reduced for the cells in both BE and BE-PPOA due to the activation process. However, $R_{ct}$ of the cell in BE is dramatically increased in the following cycles in contrast to the very stable $R_{ct}$ for the cell in BE-PPOA, which proves that PPOA additive stabilizes the Li/electrolyte interfaces. X-ray photoelectron spectroscopy (XPS) analysis was performed to characterize the compositions of the SEI layers on the Li metal anode in BE and BE-PPOA. After the Li metal was cycled in BE-PPOA, the high-resolution C 1s XPS spectrum shows that SEI film has lower amounts of C=O, C-O and $CO_3^{2-}$ than those in BE, indicating the side reactions between the solvents and Li metal are suppressed (Figure S11a-c). Besides, F 1s XPS spectra show the introduction of PPOA leads to higher LiF content in the SEI layer (Figure S11d and e), which is known to enhance the interfacial stability of Li metal anode[34, 35].

The reversibility of Li metal anode in BE-PPOA is investigated through studying the average coulombic efficiency (CE) in Li||Cu cells and electrochemical performances in full cells. The cell in BE delivers a much lower average CE (84%) compared with that in BE-PPOA (97.2%) (Figure 3a), demonstrating the consumption of Li metal by the electrolyte is effectively suppressed by the PPOA additive.

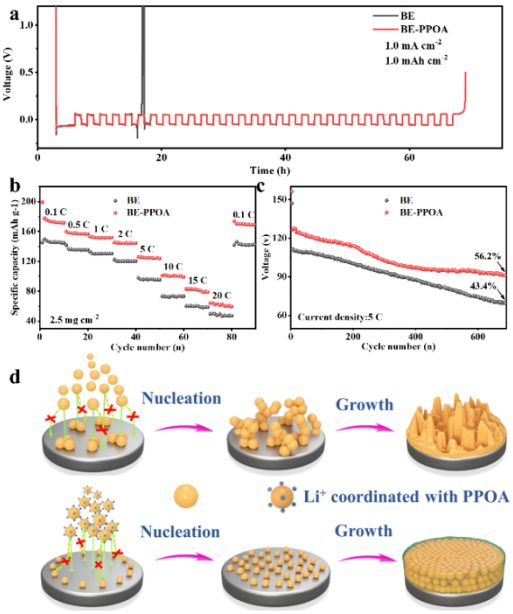


**Figure 3**. (a) Voltage-time curves of Li||Cu cells in BE and BE-PPOA with a fixed capacity of 1 mAh $cm^{-2}$ at 1 mA $cm^{-2}$. (b) Rate performance and (c) cycling stability of LTO||Li full cells in BE and BE-PPOA at 5 C (1 C=175 mA $g^{-1}$). (d) Schematic diagram of Li deposition in BE and BE-PPOA.

To further confirm the benefit of PPOA additive, the electrochemical performance of full cells assembled with lithium titanium oxide (LTO) cathode was studied. As shown in Figure S12a, the LTO||Li cell without PPOA delivers a low capacity of 146.6 mAh $g^{-1}$ with an initial CE of 89.3% (Figure S12a). In contrast, the full cell in BE-PPOA exhibits a high capacity of 172.3 mAh $g^{-1}$ with an initial CE of 86.6% (Figure S12b). The slightly decreased CE may be caused by the partial decomposition of PPOA in the first cycle, as demonstrated by a small discharge plateau at 1.65 V. With the increase in current

density, the full cell in BE-PPOA delivers higher capacities than that in BE at various current densities (Figure 3b). The LTO||Li cell in BE-PPOA shows a higher capacity of 64.1 mAh $g^{-1}$ at 20 C (Figure S12c), while the LTO||Li cell in BE only delivers a low capacity of 49.6 mAh $g^{-1}$. Besides, the capacity of LTO||Li cell in BE-PPOA can be completely recovered after the current density was reset to 0.1 C. Furthermore, the full cell with PPOA additive maintains a high specific capacity of 88.5 mAh $g^{-1}$ after 700 cycles at 5 C with a capacity retention of 56.2%, which is much higher than that in BE (Figure 3c). The enhanced stability is verified by the SEM images of cycled Li metal anode in the LTO||Li cell (Figure S13). The cycled Li metal anode in BE-PPOA still presents a smooth surface without dendrites. In contrast, the cycled Li metal anode in BE shows a porous surface.

The schematic diagram of Li deposition is shown in Figure 3d. Li ions deposit at nucleation sites in BE, resulting in the formation of individual protrusions followed by dendrite growth with the deposition going on. In contrast, the coordination between PPOA and Li ions increases the over-potential of the electrochemical deposition reaction. Therefore, significantly more nucleation sites are generated, leading to more grains gradually growing together to form a dense and smooth surface in the deposition process.

In summary, we introduced PPOA as an effective additive to improve the stability of Li metal anode in ester carbonate. The introduction of PPOA can increase the over-potential of the electrochemical deposition reaction in the initial cycle and boost the nucleation quantity to achieve a dense and smooth surface with a higher amount of LiF. As a result, the Li metal anode in both symmetric cells and full cells exhibits greatly enhanced stability and reversibility. Our work demonstrates that grain refinement via efficient additives is a promising strategy for stabilizing lithium metal batteries.

## Conflicts of interest

There are no conflicts to declare.

## Notes and references

[1] R. Zhang, N.-W. Li, X.-B. Cheng, Y.-X. Yin, Q. Zhang and Y.-G. Guo, *Advanced Science*, 2017, **4,** 1600445.
[2] C. Chen, Q. Liang, Z. Chen, W. Zhu, Z. Wang, Y. Li, X. Wu and X. Xiong, *Angewandte Chemie International Edition*, 2021, **60,** 26718-26724.
[3] H. Yang, L. Yin, H. Shi, K. He, H.-M. Cheng and F. Li, *Chemical Communications*, 2019, **55,** 13211-13214.
[4] K. Wang, L. Yang, Z. Wang, Y. Zhao, Z. Wang, L. Han, Y. Song and F. Pan, *Chemical Communications*, 2018, **54,** 13060-13063.
[5] X.-B. Cheng, R. Zhang, C.-Z. Zhao and Q. Zhang, *Chemical Reviews*, 2017, **117,** 10403-10473.
[6] G. Li, Q. Huang, X. He, Y. Gao, D. Wang, S. H. Kim and D. Wang, *ACS Nano*, 2018, **12,** 1500-1507.
[7] J. Hassoun, H.-G. Jung, D.-J. Lee, J.-B. Park, K. Amine, Y.-K. Sun and B. Scrosati, *Nano Letters*, 2012, **12,** 5775-5779.
[8] W.-K. Shin, A. G. Kannan and D.-W. Kim, *ACS Applied Materials & Interfaces*, 2015, **7,** 23700-23707.
[9] S. S. Zhang, *ACS Applied Energy Materials*, 2018, **1,** 910-920.
[10] Y. Lei, Y. Xie, Y. Huang, Q. Wang, Z. Li, X. Wu, Y. Qiao, P. Dai, L. Huang, Y. Hua, C. Wang and S. Sun, *Chemical Communications*, 2021, **57,** 10055-10058.
[11] Y. Feng, C. Zhang, X. Jiao, Z. Zhou and J. Song, *Energy Storage Materials*, 2020, **25,** 172-179.
[12] Y. Guo, H. Li and T. Zhai, *Advanced materials*, 2017, **29,** 1700007.
[13] J. Dong, H. Dai, Q. Fan, C. Lai and S. Zhang, *Nano Energy*, 2019, **66,** 104128.
[14] D. Liu, X. Xiong, Q. Liang, X. Wu and H. Fu, *Chemical Communications*, 2021, **57,** 9232-9235.
[15] X. Fan, L. Chen, X. Ji, T. Deng, S. Hou, J. Chen, J. Zheng, F. Wang, J. Jiang, K. Xu and C. Wang, *Chem*, 2018, **4,** 174-185.
[16] W. Gang, C. Chen, Y. Chen, X. Kang, C. Yang, F. Wang, Y. Liu and X. Xiong, *Angewandte Chemie International Edition*, 2019, **59,** 2055-2060.
[17] S. Ye, L. Wang, F. Liu, P. Shi, H. Wang, X. Wu and Y. Yu, *Advanced Energy Materials*, 2020, **10,** 2002647.
[18] S.-W. Ke, Y. Wang, J. Su, K. Liao, S. Lv, X. Song, T. Ma, S. Yuan, Z. Jin and J.-L. Zuo, *Journal of the American Chemical Society*, 2022, **144,** 8267-8277.
[19] T. Chen, F. Meng, Z. Zhang, J. Liang, Y. Hu, W. Kong, X. L. Zhang and Z. Jin, *Nano Energy*, 2020, **76,** 105068.
[20] T. Chen, W. Kong, P. Zhao, H. Lin, Y. Hu, R. Chen, W. Yan and Z. Jin, *Chemistry of Materials*, 2019, **31,** 7565-7573.
[21] X.-l. Huang, D. Xu, S. Yuan, D.-l. Ma, S. Wang, H.-y. Zheng and X.-b. Zhang, *Advanced Materials*, 2014, **26,** 7264-7270.
[22] Y. Liu, R. Hu, D. Zhang, J. Liu, F. Liu, J. Cui, Z. Lin, J. Wu and M. Zhu, *Advanced Materials*, 2021, **33,** 2004711.
[23] T. Chen, W. Kong, Z. Zhang, L. Wang, Y. Hu, G. Zhu, R. Chen, L. Ma, W. Yan, Y. Wang, J. Liu and Z. Jin, *Nano Energy*, 2018, **54,** 17-25.
[24] Y. Shuai, Z. Zhang, K. Chen, J. Lou and Y. Wang, *Chemical Communications*, 2019, **55,** 2376-2379.
[25] Y. Xu, H. Wu, Y. He, Q. Chen, J.-G. Zhang, W. Xu and C. Wang, *Nano Letters*, 2019, **20,** 418-425.
[26] L. Suo, W. Xue, M. Gobet, S. G. Greenbaum, C. Wang, Y. Chen, W. Yang, Y. Li and J. Li, *Proceedings of the National Academy of Sciences*, 2018, **115,** 1156-1161.
[27] F. Ding, W. Xu, G. L. Graff, J. Zhang, M. L. Sushko, X. Chen, Y. Shao, M. H. Engelhard, Z. Nie, J. Xiao, X. Liu, P. V. Sushko, J. Liu and J.-G. Zhang, *Journal of the American Chemical Society*, 2013, **135,** 4450-4456.
[28] H. Dai, K. Xi, X. Liu, C. Lai and S. Zhang, *J Am Chem Soc*, 2018, **140,** 17515-17521.
[29] Y.-X. Xie, Y.-X. Huang, X.-H. Wu, C.-G. Shi, L.-N. Wu, C. Song, J.-J. Fan, P. Dai, L. Huang, Y.-J. Hua, C.-T. Wang, Y.-M. Wei and S.-G. Sun, *Journal of Materials Chemistry A*, 2021, **9,** 17317-17326.
[30] H. Dai, X. Gu, J. Dong, C. Wang, C. Lai and S. Sun, *Nature Communications*, 2020, **11,** 643.
[31] B. Qiao, G. M. Leverick, W. Zhao, A. H. Flood, J. A. Johnson and Y. Shao-Horn, *Journal of the American Chemical Society*, 2018, **140,** 10932-10936.
[32] Q. Li, Z. Cao, W. Wahyudi, G. Liu, G.-T. Park, L. Cavallo, T. D. Anthopoulos, L. Wang, Y.-K. Sun, H. N. Alshareef and J. Ming, *ACS Energy Letters*, 2021, **6,** 69-78.
[33] R. Narayan and R. Dominko, *Nature Reviews Chemistry*, 2022, **6,** 449-450.
[34] X.-Q. Zhang, X. Chen, R. Xu, X.-B. Cheng, H.-J. Peng, R. Zhang, J.-Q. Huang and Q. Zhang, *Angewandte Chemie International Edition*, 2017, **56,** 14207-14211.
[35] Y. Yuan, F. Wu, Y. Bai, Y. Li, G. Chen, Z. Wang and C. Wu, *Energy Storage Materials*, 2019, **16,** 411-418.

 